Electronic Supplementary Information

B_3S Monolayer: Prediction of A High-Performance Anode Material for Lithium–Ion Battery

Saibal Jana [a], *Siby Thomas* [a], *Chi Ho Lee* [a], *Byeongsun Jun* [a] *and Sang Uck Lee* [a,b]

[a] Department of Bionano Technology and [b] Department of Chemical and Molecular Engineering,
Hanyang University, Ansan 15588, Republic of Korea

(Email : saibal@cms.hanyang.ac.kr, sulee@hanyang.ac.kr)

CONTENTS

Calculation Details 2

Fig. S1. Optimized low-lying energy geometries of B_3S monolayer 4

Fig. S2 The in-plane polar diagrams for (a) Young's modulus, and (b) Poisson ratio along an arbitrary direction θ of the B_3S monolayer 5

Fig. S3. Li adsorption energy obtained using PSO algorithm at different concentration of Li atom. Here x represents the Li concentration. The inset structures are of Li_0B_3S, Li_2B_3S, and Li_4B_3S. 6

Fig. S4. Fluctuations of total potential energy of lithiated B_3S monolayer during the AIMD simulations at 300 K. The inset is the structure of lithiated B_3S monolayer at the end of the AIMD simulation (a) full lithiation at one side of the B_3S monolayer (b) full lithiation at both side of the B_3S monolayer. 7

Fig. S5. (a) Li diffusion energy barrier, where other side of the B_3S monolayer is fully lithiated. (b) Vacancy diffusion barrier, where other side of the B_3S monolayer is fully lithiated. 8

Table S1. Summary of theoretical specific capacities (mA h g^{-1}) of some widely investigated promising anode materials for LIBs 9

References 10

Calculation Details:

Structure of the B_3S was generated and optimized using CALYPSO code and VASP respectively. 2 × 2 supercell structure is considered with 30 Å vacuum distance in C direction with 3 × 3 × 1 k-point grid according to the Monkhorst-Pack scheme. The kinetic energy cut off is 700 eV. The energy and atomic forces convergence criteria are set at 10^{-6} eV and 10^{-3} eV/Å for geometry relaxation. *Ab initio* molecular dynamics (AIMD) simulations in NVT ensemble lasted for 5 ps. The force calculated in the Phonopy code using LDA potential. The in-plane Young's modulus and Poisson ratio along different θ direction relative to the positive x-direction can be expressed as

$$E(\theta)=\frac{C_{11}C_{22}-C_{12}{}^{2}}{C_{11}\sin^4\theta+C_{22}\cos^4\theta+\left(\frac{C_{11}C_{22}-C_{12}{}^{2}}{C_{44}}-2C_{12}\right)\cos^2\theta\sin^2\theta} \tag{S1}$$

$$\nu(\theta)=\frac{\left(C_{11}+C_{22}-\frac{C_{11}C_{22}-C_{12}{}^{2}}{C_{44}}\right)\cos^2\theta\sin^2\theta-C_{12}\left(\cos^4\theta+\sin^4\theta\right)}{C_{11}\sin^4\theta+C_{22}\cos^4\theta+\left(\frac{C_{11}C_{22}-C_{12}{}^{2}}{C_{44}}-2C_{12}\right)\cos^2\theta\sin^2\theta} \tag{S2}$$

The calculated E(θ) and ν(θ) of B_3S monolayer are depicted in the polar diagrams in Fig. S2. From the diagram, it can be said that both Young's modulus and Poisson ratio are anisotropic in nature. Specific capacity is calculated by introducing the Li using CALYPSO code again. To get average open circuit voltage CASM code is used. And Li diffusion barrier computed using the climbing image nudged elastic band (CI-NEB) method interface with VASP.

To understand the environmental effect from other side of the monolayer on the diffusion, we have performed Li and vacancy diffusion in one side when other side is fully lithiated at low and high

SOC. The Li diffusion path for the system with other side fully lithiated geometry is A_1 → A_2 → A_1 → A_1 (Fig. S5a). Here, Li at A_2 site is very much unstable due to the increment of the distance between the Li atom and monolayer from 1.72 to 1.76 Å at one side and both side lithiated geometry respectively. Therefore, the p_z orbital of the B atom, a responsible factor for the Li atom stability through the formation of non-covalent interaction with Li atom is at the far positon resulting the instability of Li atom at A_2 site. Therefore, no suitable path is observed in between A_1 and A_2 sites, but considerable barrier of 0.33 eV is present between two neighboring A_1 sites. And for high state of charge the diffusion of the vacancy is calculated. The single vacancy at A_2 site is most stable compare to the A_1 sites. Here, stability of the vacant neighboring A_1 sites is different due the puckered geometry in presence of Li at both side of the B_3S monolayer. For the easy understanding, here we have considered two neighboring A_1 sites as A_{1a} and A_{1b} (Fig. S5b). If the vacancy is in A_{1a} then the Li atom at A_{1b} is close to the boron plane (1.63 Å) and form stable geometry. Again, the vacancy at A_{1b}, i.e. Li atom at A_{1a} is far away from boron plane (1.79 Å) due to puckered orientation is less stable. Here, the calculated vacancy diffusion barrier for the pathways A_2 → A_1 → A_1 → A_2 are 0.53, 0.18, and 0.28 eV respectively.

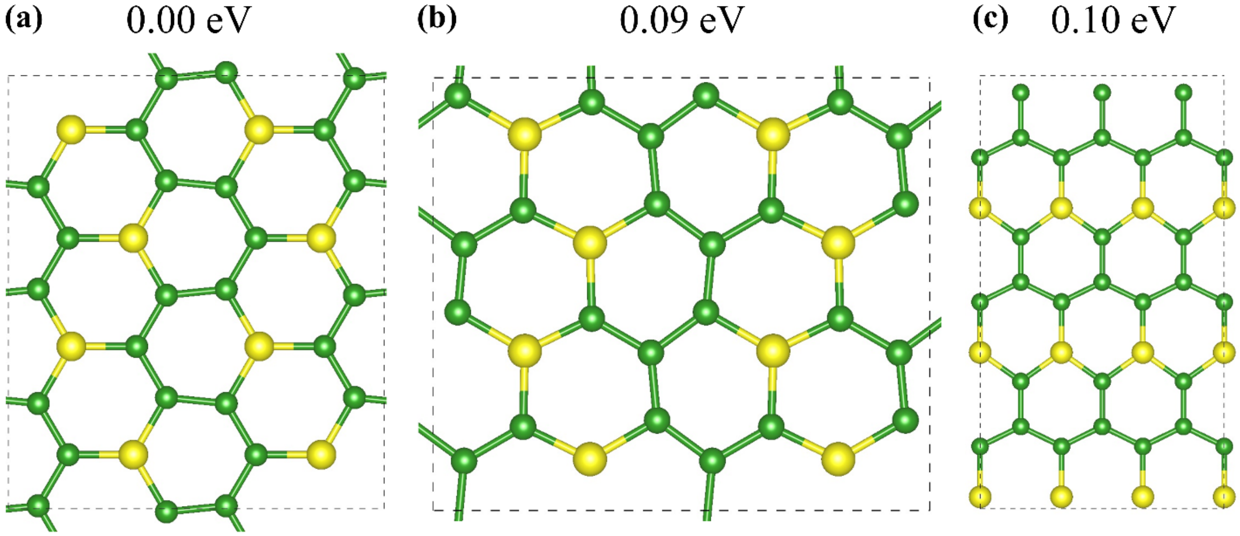

Fig. S1. Optimized low-lying energy geometries of B_3S monolayer

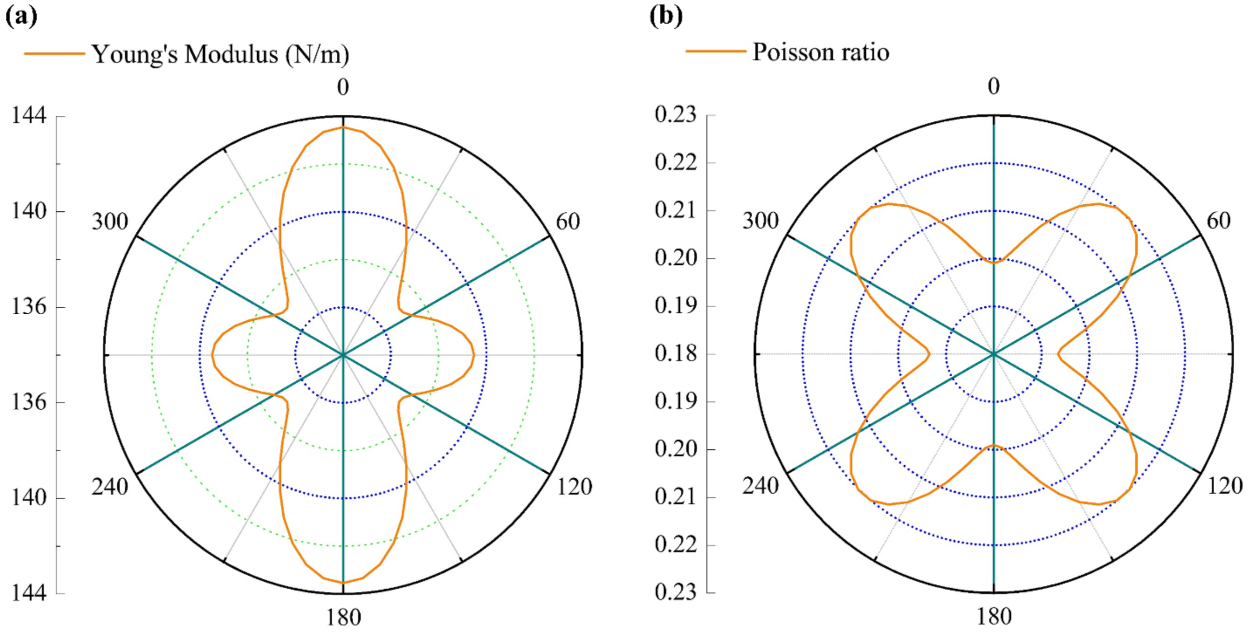

Fig. S2. The in-plane polar diagrams for (a) Young's modulus, and (b) Poisson ratio along an arbitrary direction θ of the B_3S monolayer.

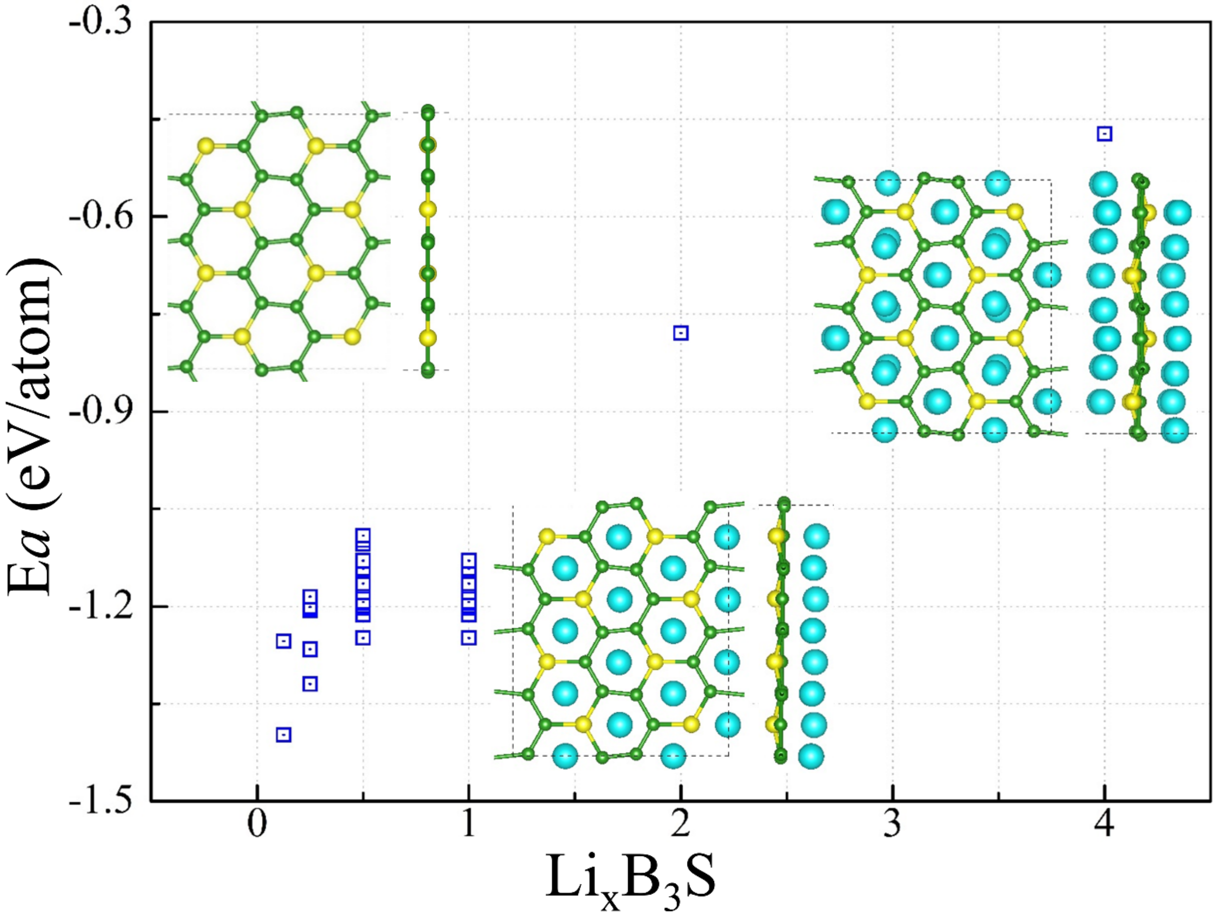

Fig. S3. Li adsorption energy obtained using PSO algorithm at different concentration of Li atom. Here x represents the Li concentration. The inset structures are of Li_0B_3S, Li_2B_3S, and Li_4B_3S (top and side view).

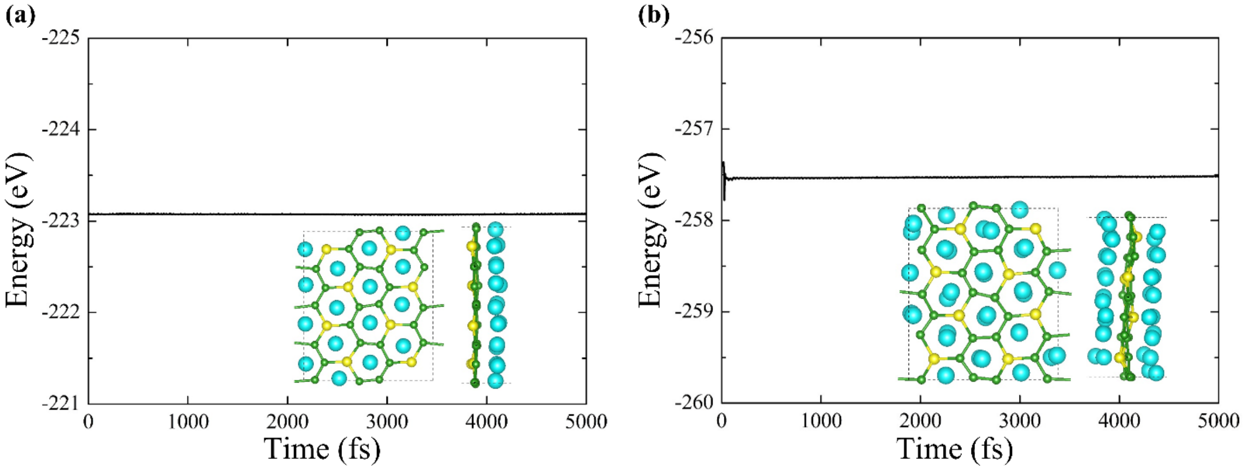

Fig. S4. Fluctuations of total potential energy of lithiated B_3S monolayer during the AIMD simulations at 300 K. The inset is the structure of lithiated B_3S monolayer at the end of the AIMD simulation (a) full lithiation at one side of the B_3S monolayer (b) full lithiation at both side of the B_3S monolayer.

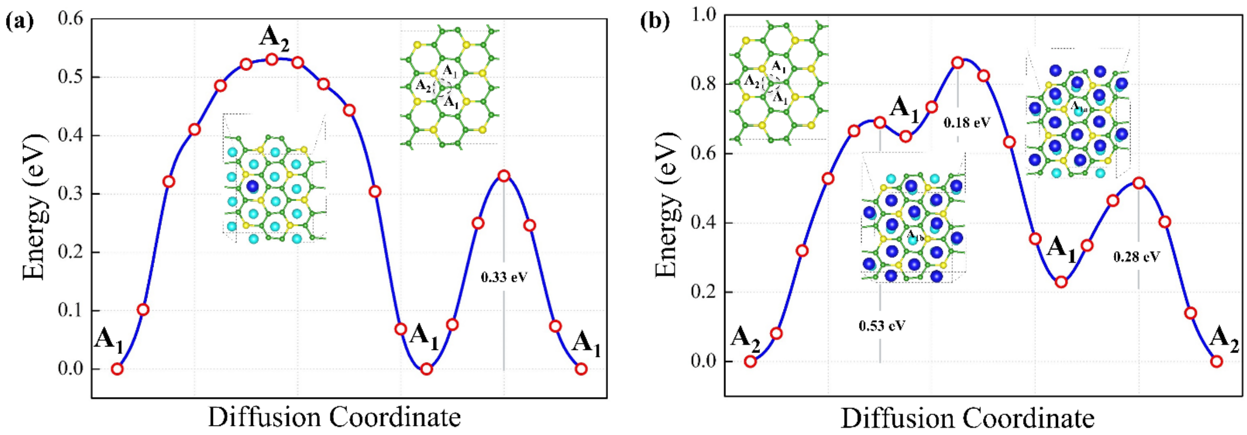

Fig. S5. (a) Li diffusion energy barrier, where other side of the B_3S monolayer is fully lithiated.

(b) Vacancy diffusion barrier, where other side of the B_3S monolayer is fully lithiated.

Table S1. Summary of theoretical specific capacities (mA h g^{-1}) of some widely investigated promising anode materials for LIBs

2D monolayer	Theoretical Capacity (mA h g^{-1})
B_3S	**1662** (this work)
1T-Ti_3C_2	320[1]
Graphite	372[2]
Ψ-Graphene	372[3]
2D-Boron	383[4]
Phosphorene	433[5]
Orthorhombic Mo_2B_2	444[6]
2D-Ti_2B_2	456[7]
VS_2	466[8]
B_2H_2	504[9]
1H-Mo_2C	526[10]
Phagraphene	558 [11]
2D-TiB_4	588 [12]
Orthorhombic Fe_2B_2	665[6]
MoS_2	670[13]
Mn_2C	879 [14]
V_2C	940 [15]
Silicene	954 [16]
TiC_3	1278[17]
BP	1283[18]
Popgraphene	1487 [19]
B_2S	1498[20]
g-SiC_3	2090[21]

References:

1. Q. Tang, Z. Zhou and P. Shen, *J. Am. Chem. Soc.*, 2012, **134**, 16909-16916.
2. M. Winter, J. O. Besenhard, M. E. Spahr and P. Novak, *Adv. Mater.*, 1998, **10**, 725-763.
3. X. Y. Li, Q. Wang and P. Jena, *J. Phys. Chem. Lett.*, 2017, **8**, 3234-3241.
4. S. Banerjee, G. Periyasamy and S. K. Pati, *J. Mater. Chem. A*, 2014, **2**, 3856-3864.
5. S. J. Zhao, W. Kang and J. M. Xue, *J. Mater. Chem. A*, 2014, **2**, 19046-19052.
6. Z. L. Guo, J. Zhou and Z. M. Sun, *J. Mater. Chem. A*, 2017, **5**, 23530-23535.
7. T. Bo, P. F. Liu, J. P. Xu, J. R. Zhang, Y. B. Chen, O. Eriksson, F. W. Wang and B. T. Wang, *Phys. Chem. Chem. Phys.*, 2018, **20**, 22168-22178.
8. Y. Jing, Z. Zhou, C. R. Cabrera and Z. Chen, *J. Phys. Chem. C*, 2013, **117**, 25409-25413.
9. N. K. Jena, R. B. Araujo, V. Shukla and R. Ahuja, *ACS Appl. Mater. Interfaces*, 2017, **9**, 16148-16158.
10. Q. L. Sun, Y. Dai, Y. D. Ma, T. Jing, W. Wei and B. B. Huang, *J. Phys. Chem. Lett.*, 2016, **7**, 937-943.
11. Z. H. Wang, X. F. Zhou, X. M. Zhang, Q. Zhu, H. F. Dong, M. W. Zhao and A. R. Oganov, *Nano Lett.*, 2015, **15**, 6182-6186.
12. X. Qu, J. H. Yang, Y. C. Wang, J. Lv, Z. F. Chen and Y. M. Ma, *Nanoscale*, 2017, **9**, 17983-17990.
13. L. Zhang, H. B. Wu, Y. Yan, X. Wang and X. W. Lou, *Energy Environ. Sci.*, 2014, **7**, 3302-3306.
14. Y. G. Zhou and X. T. Zu, *Electrochim. Acta*, 2017, **235**, 167-174.
15. J. P. Hu, B. Xu, C. Y. Ouyang, S. Y. A. Yang and Y. G. Yao, *J. Phys. Chem. C*, 2014, **118**, 24274-24281.
16. G. A. Tritsaris, E. Kaxiras, S. Meng and E. G. Wang, *Nano Lett.*, 2013, **13**, 2258-2263.
17. T. Yu, Z. Y. Zhao, L. L. Liu, S. T. Zhang, H. Y. Xu and G. C. Yang, *J. Am. Chem. Soc.*, 2018, **140**, 5962-5968.
18. H. R. Jiang, W. Shyy, M. Liu, L. Wei, M. C. Wu and T. S. Zhao, *J. Mater. Chem. A*, 2017, **5**, 672-679.
19. S. W. Wang, B. C. Yang, H. Y. Chen and E. Ruckenstein, *J. Mater. Chem. A*, 2018, **6**, 6815-6821.
20. P. Li, Z. Y. Li and J. L. Yang, *J. Phys. Chem. Lett.*, 2018, **9**, 4852-4856.
21. X. S. Lv, W. Wei, B. B. Huang and Y. Dai, *J. Mater. Chem. A*, 2019, **7**, 2165-2171.